Piezoelectric Energy Harvesting from a Composite Cantilever Beam under Sinusoidal Excitation

Modeling and Experimental Verification

Theofanis Plagianakos, Nikolaos Margelis, Nikolaos Leventakis, Georgios Bolanakis, Panagiotis Vartholomeos and Evangelos Papadopoulos
Control Systems Lab, School of Mechanical Engineering, National Technical University of Athens, Athens, Greece
egpapado@central.ntua.gr

***Abstract*—Modeling and experimental verification of energy harvesting for a composite cantilever beam with a piezoelectric patch are presented. Finite element and lumped-parameter models are developed for open- and closed resistive circuit. A basic in-house circuit is compared to a commercial one in terms of power output. Results indicate good performance of the lumped-parameter models. The effect of frequency on the harvested power is also presented.

Keywords—piezoelectric; harvesting; composite materials.

I. Introduction

In the last two decades, piezoelectric energy harvesting (PEH) for feeding low-power devices has become an emerging research field [1]-[2]. Its main applications include exploitation of the energy produced by human motion or ambient vibration in order to provide power in the range of mW to electronic equipment in the context of IoT solutions [3]-[5]. The energy that can be harvested using PEH is still limited to the range of a few tens of microwatts to a few milliwatts. This low power output necessitates not only the design of ultra-low power logic circuits but also of efficient power delivery circuits that maximize the available power out of the energy harvesters.

The simplest configuration of PEH comprises the piezoelectric element, an ac-dc diode rectifier, smoothing capacitor and a switch-mode dc-dc converter to provide the dc power to the load [6]-[7]. Ottman developed an adaptive circuit that adjusts the sourced current to increase the power transfer [8]. However, adaptive circuits rely on closed-loop control and need complex electronic interfaces, which dramatically reduce the efficiency of the energy harvester. These limitations are addressed by the authors in [9] using a low-power single-chip analog controller. A different approach is based on the Synchronized Switch Harvesting on Inductor (SSHI) technique [10]-[11], which employs an inductor in combination with the PEH capacitor, so that the energy to charge the capacitor necessary to conduct the following rectifier diode(s) can be harvested, which would otherwise have been wasted.

The piezoelectric models in the literature, used for predicting power transfer and tuning controllers, include coupled single degree-of-freedom (SDOF) models [12]-[13], exact analytical solutions [14], approximate distributed parameter models (Rayleigh–Ritz method) [15], and distributed parameter modeling approaches [16] that consider a single vibration mode. Distributed parameter elements have a relatively low computational cost and offer fast and reliable solutions for dynamic operations. While finite element models are used often for validation of the vibration response of the open-circuit electromechanical system, a limited number of them can be used to simulate the closed-circuit response [17].

The present work aims at presenting ongoing progress on modeling and testing PEH systems on a composite beam with a piezoelectric patch. Continuum and lumped-parameter models are developed and validated against measurements. Also, an in-house developed harvesting circuit (IHHC) is compared with a commercial solution (CHC) in terms of power output.

II. Continuum and Lumped Parameter Models

The composite beam with the PP employed are shown in Fig. 1. The relevant dimensions are L=233 mm, b=35 mm, h=2.15 mm, L_p=50 mm and b_p=30 mm.

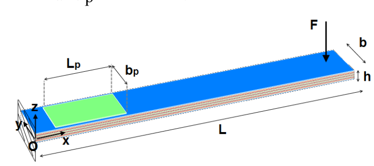

Fig. 1. Geometry of composite beam with patch.

The piezoelectric material is assumed to be polarized along its thickness, perfectly bonded to the composite substrate and to exhibit linear piezoelectric behavior. The ply constitutive equations in the natural coordinate system Oxyz have the form:

$$\begin{aligned}\boldsymbol{\sigma}_i &= C_{ij}^{E}\mathbf{S}_j - \left(e_{mi}\right)^T \mathbf{E}_m \\ \mathbf{D}_m &= e_{mj}\mathbf{S}_j + \varepsilon_{mm}^{S}\mathbf{E}_m\end{aligned} \tag{1}$$

where i,j=1,…,6 and m=1,…,3; $\boldsymbol{\sigma}_i$ and $\mathbf{S}_j$ are the mechanical stress and engineering strain in vectorial notation; $\mathbf{E}_m$ is the electric field vector; $\mathbf{D}_m$ is the electric displacement vector; C_{ij} is the elastic stiffness tensor; e_{mj} is the piezoelectric tensor arising from the piezoelectric charge tensor and the stiffness tensor; and ε_{mm} is the material electric permittivity tensor. Superscripts E and S indicate constant electric field and strain conditions, respectively. Eq. (1) is valid for arbitrary laminate

This research has been co-financed by the European Regional Development Fund of the European Union and Greek national funds through the Operational Program Competitiveness, Entrepreneurship and Innovation, under the call RESEARCH – CREATE – INNOVATE (project code: T1EDK-01533).

material, as it covers the behavior of both a piezoelectric and a passive composite ply (e_{mj}=0). The indices in (1) denote that the present continuum models account for the full representation of the stress and strain tensors in 3D space and may be applied to arbitrary geometries, laminations and sensor configurations. Implementation in commercial FE software occurs in a "one-shot" simulation approach, since the composite beam and the electric circuit are solved within the same model.

To validate the continuum models and extend predictions to circuitries with MOSFETS and control schemes, lumped parameter models have been developed. A basic model, see Fig. 2, includes a rotational spring, an inertia and a gyrator with properties derived from FE predictions and measurements. The lumped parameter models were implemented in Simscape [18].

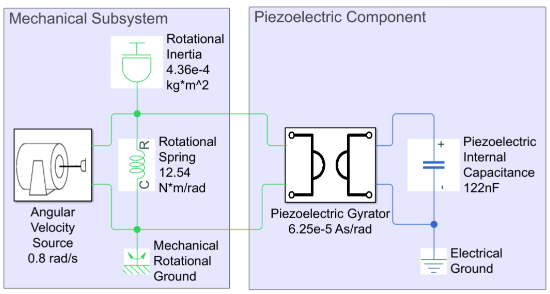

Fig. 2. Basic lumped-parameter model.

III. Experimental Configuration

The experimental setup is shown in Fig. 3. The harvested energy is provided by a P876A12 DuraAct patch from PI [19], glued on the beam upper surface at 15 mm distance from the clamped end. An LDS V201 (B&K) shaker is used to excite the specimen through a stinger instrumented with a load cell (PCB). The load cell is fixed on the specimen near the free end by a screw, nut and washer. Additional signals are acquired by an accelerometer (PCB), a piezopolymer sensor (DT1-028K from Measurement Specialties) and a current sensor with adjustable range (nA, μA or mA). All signals are collected by a BNC-2110 block and a NI PCI-6036E DAQ board. Labview software is used for providing the excitation signal (amplified by LDS LPA100 (B&K)) and measurement storage.

Four configurations were considered: (i) open circuit, (ii) closed circuit with resistive load of 12 kΩ, (iii) IHHC with diode rectifier, capacitor and a switch for capacitor discharging towards a resistive load, (iv) CHC (STMicroelectronics). The current proof of harvesting concept focuses on a frequency excitation range up to 10 Hz. Thus, sinusoidal excitation has been applied at 1 Hz and 10 Hz, respectively.

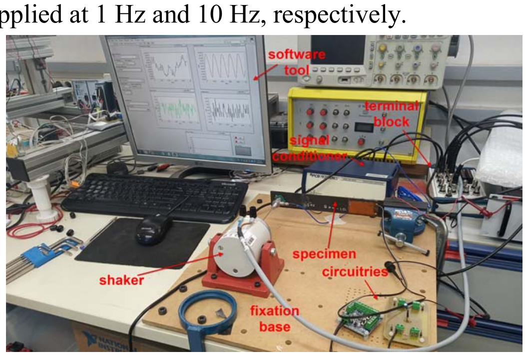

Fig. 3. Experimental configuration.

IV. Results and Discussion

The beam material is an aerospace graphite/epoxy composite M21/T800 by Hexcel with lamination $[-45/45/90_2/0/90]_S$. The composite ply properties used in the FE models were validated by measurements of the fundamental bending frequency. The piezoelectric properties are provided by the manufacturer of PIC255, which is used in the PP [19]. All material properties are listed in Table 1.

TABLE I. Material properties.

Property	**Composite Material**	**Piezoelectric Material**
Density (kg/m^3)	1554	7800
Elastic Properties		
E_{11} (GPa)	138.4	62.1
E_{22} (GPa)	8.5	62.1
E_{33} (GPa)	8.5	48.3
G_{12} (GPa)	4.3	23.2
G_{13} (GPa)	4.3	21.3
G_{23} (GPa)	4.3	21.3
ν_{12}	0.31	0.33
ν_{13}	0.31	0.43
ν_{23}	0.31	0.43
Piezoelectric Properties		
d_{31} (10^{-12} m/V)	-	-191
d_{32} (10^{-12} m/V)	-	-191
d_{33} (10^{-12} m/V)	-	409
Dielectric Properties (ε^0=8.85 10^{-12} F/m)		
$\varepsilon_{33}/\varepsilon^0$	3.5	1832

Two types of finite elements have been considered in COMSOL [20]: a 3D solid tetrahedral element with linear shape functions and a linear layerwise 2D shell element with quadratic shape functions. A total of 10635 and 435 elements have been used for the 3D and the 2D models, respectively. The PP open-circuit configuration has been considered for validation of i) the piezoelectric material properties and ii) the continuum modeling approach. Fig. 4 shows predicted and measured electric potential at the DuraAct PP terminals for the excitation frequencies considered. The force amplitude has been 0.9 N and 0.6 N at 1 Hz and 10 Hz, respectively. The measured signal reveals non-linearity, probably due to shaker stinger bending. The FE model assumes a rigid stinger and thus overestimates the strain energy converted in the sensor. The 2D shell FE yields better estimations of the measured response in terms of voltage amplitude compared to the 3D solid. This is expected, as the beam thickness aspect ratio is high (L/h=108) and would require a very dense mesh of solid elements to accurately simulate the flexibility of the beam.

A 12 kΩ resistor was connected at the terminals of the PP for determining the power converted to heat in the electric resistance. Fig. 5 shows predicted and measured values for the electric potential and current at the resistor terminals for load amplitudes 0.6 N at 1 Hz and 0.7 N at 10 Hz. As in the open-circuit case, non-linear response in the measurements may be observed, whereas noise is obvious in the current measurement at 1 Hz. The predictions of the lumped-parameter model practically coincide with the measured response. The continuum models overestimate voltage and current, probably due to element type and mesh of the thin patch, numerical solution parameters and stinger flexibility. The small values of electric current highlight the deviations, as circuit losses and noise may also affect the response. The electric power loss at the resistance may be derived from the measurements being 0.11µW at 1Hz and 10.3 µW at 10 Hz.

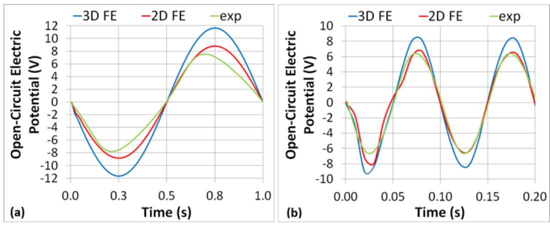

Fig. 4. Open circuit measured & predicted voltage in (a) 1 Hz , (b) 10 Hz.

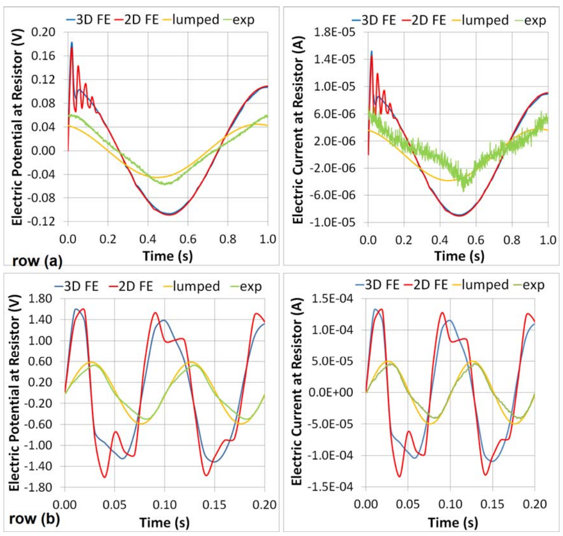

Fig. 5. Closed circuit measured & predicted voltage in (a) 1 Hz , (b) 10 Hz.

The in-house harvesting circuit, see Fig. 6, consists of a diode rectifier due to the alternating input current, a capacitor which charges accumulating electric current and a load with a switch which discharges the capacitor.

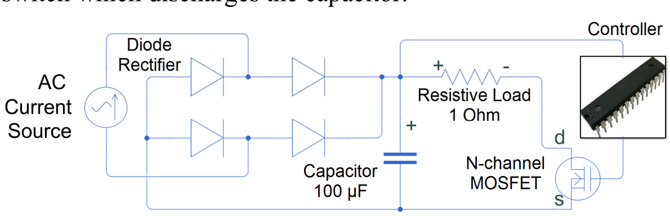

Fig. 6. Schematic diagram of the IHHC.

In Figs. 7-8 the response predicted via the lumped-parameter model is in good agreement with measurements. The circuit has been designed to charge the capacitor up to 2.4 V and then discharge completely, supplying electric charge to the load.

To evaluate and compare harvesting efficiency to that of the IHHC, experiments have been conducted based on a commercially available solution. More specifically, the STEVAL-ISV020V1 evaluation board for the SPV1050 energy harvester and battery charger have been used. The SPV1050 is an ultralow power, high-efficiency energy harvester and battery charger, which implements the maximum power point tracking function (MPPT) and integrates the switching elements of a buck-boost converter. The SPV1050 lacks the rectifying stage needed for piezoelectric sources, as it is intended for PV applications. Thus, a full-wave rectifier has been designed and implemented. The experimental setup consists of a PP connected to the full-wave rectifier, the output of which is provided directly to the evaluation board. Finally, a single-cell LiPO battery is connected to the board's output. Throughout the experiments mentioned next, the available low-dropout regulators (LDOs) have been disabled, leaving the battery charging and MPPT functions enabled.

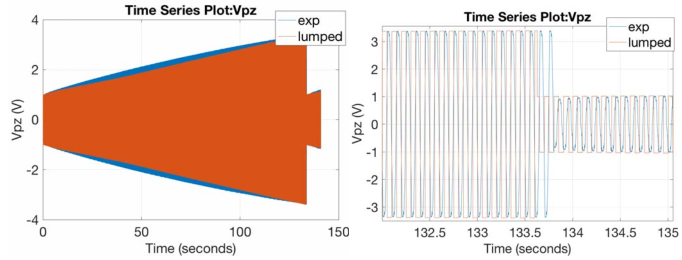

Fig. 7. Experimental and simulated (lumped parameter) voltage at the IHHC PP. Full duration (left), and zoom-in at capacitance discharge (right).

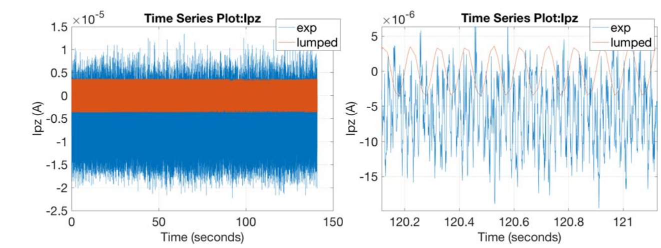

Fig. 8. Experimental and simulated (lumped parameter) current from the IHHC PP: full duration of simulation (left) and zoom-in (right).

Experiments were conducted varying the PP applied force frequency, f, and amplitude, F_A. Measurements of the charging current, Io, and the battery terminal voltage, Vb, are shown in Fig. 9. For f = 10 Hz and F_A = 0.7 N, an average output power of 71 µW was measured, while for f = 1 Hz and F_A = 1.25 N no electrical energy could be harvested since the harvesting module could not be initialized properly. Increasing the rectifier output capacitance might help override this; future experiments will be conducted to validate this assumption. Note that for f = 10 Hz and F_A = 0.7 N, the CHC was able to harvest 28.9 times more power compared to the IHHC, mainly due to the discrete components used in the latter. The energy consumed in the attached electric circuits was not measured.

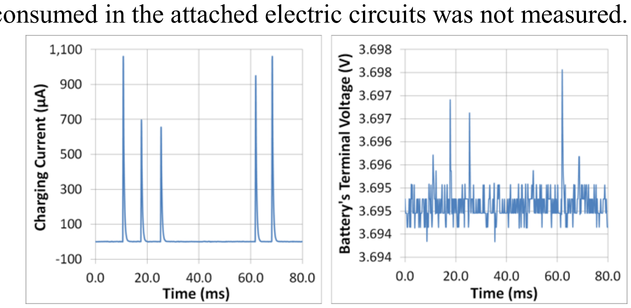

Fig. 9. Measured output current and battery voltage for 10Hz 0.7N.

V. Conclusion and Future Work

Preliminary modeling validation studies with experiments showed that the continuum models seem to overestimate the power produced by the electromechanical system in the case of a resistive circuitry. Regarding circuit development, the comparison with a commercial solution revealed the major role of parasitic losses for the studied range of power. The major effect of excitation frequency of the system has been quantified. Future work will focus on extending continuum and lumped-parameter models to non-linear mechanical response.

REFERENCES

[1] A. Erturk and D. J. Inman, *Piezoelectric Energy Harvesting*, John Wiley and Sons Ltd, UK, 2011.

[2] M. Safaei, H. A. Sodano, and S. R. Anton, "A review on energy harvesting using piezoelectric materials: state-of-the-art a decade later (2008-2018)", *Smart Mater. Struct.*, vol. 28, no. 11, pp. 1-63, November 2019.

[3] P. D. Mitcheson, E. M. Yeatman, G. Kondala Rao, A. S. Holmes and T. C. Green, "Energy harvesting from human and machine motion for wireless electronic devices", *Proc. IEEE*, vol. 96, no. 9, pp. 1457-1486, September 2008.

[4] K. A. Cook-Chennault, N. Thambi and A. M. Sastry, "Power MEMS portable devices – a review of non-regenerative and regenerative power supply systems with special emphasis on piezoelectric energy harvesting systems", *Smart Mater. Struct.*, vol. 17, no. 4, pp. 1-33, August 2008.

[5] H. S. Kim, J. H. Kim and J. Kim, "A review on piezoelectric energy harvesting based on vibration", *Int. J. Precis. Eng. Man.*, vol. 12, no. 6, pp. 1129-1141, December 2011.

[6] J. Kymissis, C. Kendall, J. Paradiso, and N. Gerhenfeld, "Parasitic power harvesting in shoes," in *Proc. 2nd Int. Symp. Wearable Comput.*, Pittsburgh, PA, Oct. 19–20, 1998, pp. 132–139.

[7] J. M. Rabaey, M. J. Ammer, J. L. da Silva Jr, D. Patel, and S. Roundy, "PicoRadio supports ad hoc ultra-low power wireless networking," *Comput.*, vol. 33, no. 7, pp. 42–48, July 2000.

[8] G. K. Ottman, H. F. Hofmann, A. C. Bhatt and G. A. Lesieutre, "Adaptive piezoelectric energy harvesting circuit for wireless remote power supply", *IEEE T Power Electr*, vol. 17, pp. 669-676, September 2002.

[9] A. Tabesh and L. G. Frechette, "A low-power stand-alone adaptive circuit for harvesting energy from a piezoelectric micropower generator," *IEEE T Ind Electron*, vol 57, iss. 3, pp. 840-849, March, 2010.

[10] D. Guyomar, A. Badel, E. Lefeuvre, and C. Richard, "Toward energy harvesting using active materials and conversion improvement by non-linear processing," *IEEE T Ultrason Ferr*, vol. 52, no. 4, pp. 584–595, April 2005.

[11] Y. K. Ramadass and A. P. Chandrakasan, "An efficient piezoelectric energy harvesting interface circuit using a bias-flip rectifier and shared inductor," *IEEE J Solid-St Circuits*, vol. 45, no. 1, January 2010.

[12] S. Roundy, P. K. Wright and J. M. Rabaey, "A study of low level vibrations as a power source for wireless sensor nodes," *Comput Commun*, vol. 26, no. 11, pp. 1131–1144, July 2003.

[13] N. E. duToit, B. L. Wardle and S. Kim, "Design considerations for MEMS-scale piezoelectric mechanical vibration energy harvesters," *Integr. Ferroelectr.*, vol. 71, no. 1, pp. 121–160, August 2005.

[14] A. Erturk and D. J. Inman, "A distributed parameter electromechanical model for cantilevered piezoelectric energy harvesters," *J Vib Acoust*, vol. 130, no. 4, 15 pages, August 2008.

[15] F. Lu, H. P. Lee and S. P. Lim, "Modeling and analysis of micro piezoelectric power generators for micro-electromechanical-systems applications," *Smart Mater Struct*, v. 13, n. 1, pp. 57–63, February 2004.

[16] S. N. Chen, G. J. Wang and M. C. Chien, "Analytical modeling of piezoelectric vibration-induced micro power generator," *Mechatronics*, vol. 16, no. 7, pp. 397–387, September 2006.

[17] H. Wang, X. Shan and T. Xie, "Performance optimization for cantilevered piezoelectric energy harvester with a resistive circuit", *Proc. of 2012 IEEE ICMA*, Chengdu, China, August 5-8, 2012.

[18] Mathworks, *SimscapeTM User's Guide (2020a),* 2020.

[19] PI Ceramic GmbH, *Piezoelectric Ceramic Products*, 2020.

[20] Comsol AB, *Comsol Multiphysics Reference Manual*, v. 5.5, 2019.